Soft Matter

Dynamics and Thermodynamics of Air-Driven Active Spinners

Journal:	*Soft Matter*
Manuscript ID	SM-ART-02-2018-000403.R1
Article Type:	Paper
Date Submitted by the Author:	22-May-2018

Complete List of Authors:	Farhadi, Somayeh; University of Pennsylvania, Machaca, Sergio; Drexel University Aird, Justin; Virginia Polytechnic Institute and State University Torres Maldonado, Bryan; University of Puerto Rico at Mayagüez Davis, Stanley Davis; Hampton University Arratia, Paulo; University of Pennsylvania, Mechanical Engineering and Applied Mechanics Durian, Douglas; University of Pennsylvania, Physics & Astronomy

Journal Name

ARTICLE TYPE

Cite this: DOI: 10.1039/xxxxxxxxxx

Dynamics and Thermodynamics of Air-Driven Active Spinners†

Somayeh Farhadi,*[a] Sergio Machaca,[a,b] Justin Aird,[a,c] Bryan O. Torres Maldonado,[a,d] Stanley Davis,[a,e] Paulo E. Arratia,*[a] and Douglas J. Durian, *[a]

Received Date
Accepted Date

DOI: 10.1039/xxxxxxxxxx

www.rsc.org/journalname

We report on the collective behavior of active particles in which energy is continuously supplied to rotational degrees of freedom. The *active spinners* are 3D-printed disks, 1 cm in diameter, that have an embedded fan-like structure, such that a sub-levitating up-flow of air forces them to spin. Single spinners exhibit Brownian motion with a narrow Gaussian velocity distribution function, $P(v)$, for translational motion. We study the evolution of $P(v)$ as the packing fraction and the average single particle spin speeds are varied. The interparticle hydrodynamic interaction is negligible, and the dynamics is dominated by hyperelastic collisions and dissipative forces. As expected for nonequilibrium systems, $P(v)$ for a collection of many spinners deviates from Gaussian behavior. However, unlike translationally active systems, phase separation is not observed, and the system remains spatially homogeneous. We then search for a near-equilibrium counterpart for our active spinners by measuring the equation of state. Interestingly, it agrees well with a hard-sphere model, despite the dissipative nature of the single particle dynamics.

Introduction

Systems that contain self-propelling particles are ubiquitous and span a wide range of length scales[1], from flocking of birds (∼km) to motile ants (∼m) to swimming of microorganisms (∼ μm). These active systems are characterized by self-propelling units or particles that can either store or acquired energy from their environment, generate mechanical stresses, and create flows within the fluid medium. Examples include living organisms[1,2] and self-propelled colloids[1,3–5,5–12], as well as shaken[13–19] and air-fluidized[20–28] granular particles. Active systems displays properties not seen in their passive counterparts such as large-scale flows[2], anomalous rheological properties[29], and giant density fluctuations[16,25]. These unusual properties are currently being exploited for potential applications in medicine, robotics, and energy harvesting[1,30,31], and as a result active systems have gained substantial attention over the past decade or so. Despite different motility mechanisms, a unifying feature of active systems is their out of equilibrium collective dynamics, where a thermodynamic-based description usually (but not always[20–23,27,28]) fails to exist. As a result, finding a framework to describe the bulk properties of active matter remains as a challenge.

While active particles can both translate and rotate, the majority of previous studies focus on translational activity, in which the energy input directly results in linear momentum gain[1]. The dynamics of rotationally active particles, on the other hand, has been far less explored and only a few experimental studies are available. Colloidal micro-rollers are an example of such particles, where particle rotation is induced by external magnetic torque[3,12,32]. These colloidal particles have shown many fascinating collective behavior including self-assembly, crystal formation, and melting[9]. An important question is to what extent these behavior is due to rotational activity in contrast to hydrodynamic interaction, which is known to play an important role in colloidal systems[4,12].

An early simulation[33] suggested that rotational activity without hydrodynamic interactions indeed maintains spatial homogeneity (unlike the typical phase separation observed in active systems[1]). That study[33] also found that while the particle rotational speed distribution, $P(\omega)$, is Maxwellian, the translational $P(v)$ deviates from Maxwell-Boltzmann description, in agreement with a recent experiment[34]. Other studies on rotational activity without hydrodynamic interactions demonstrated conflicting results. For instance, simulations of concave-shaped spinners by[35] showed spontaneous phase separation and the coexistence of self-organized substructures. The accompanying paper by Workamp *et al.* shows that the geometric friction between colliding particles

[a] *University of Pennsylvania, Philadelphia, PA 19104, USA*
[b] *Drexel University, Philadelphia, PA 19104, USA*
[c] *Virginia Polytechnic Institute and State University, Blacksburg, VA 24061, USA*
[d] *University of Puerto Rico at Mayagüez, San Juan, Puerto Rico*
[e] *Hampton University, Hampton, VA 23668, USA*
* *Corresponding Authors*

† Electronic Supplementary Information (ESI) available: [details of any supplementary information available should be included here]. See DOI: 10.1039/b000000x/

plays an important role in their collective dynamics. The latter two studies suggest that the details of angular momentum transfer in particle-particle collisions, even in the absence of hydrodynamic interactions, is an important determinant for the collective behavior in rotationally active particles.

Granular gases are a classic example of active matter, where the hydrodynamic interactions are absent in particle dynamics. The dynamics of vibrated granular gases have been studied in details over the past two decades. Several independent studies found that velocity distribution functions, $P(v)$, of granular gases have a central part which behaves as $\exp[-|v|^{3/2}]$ or $\exp[-v^2]$ depending on the driving mechanism, and tails which fall either exponentially $\exp[-|v|/v_c]$, or as an stretched exponential $\exp[-|v/v_c|^{\beta}]$ [15,19,36–42]. Note that any deviation of $P(v)$ from Gaussian form indicates out of equilibrium dynamics which impacts the possibility of a thermodynamic description for the system. A natural question that rises is whether and how rotational activity impacts the form of $P(v)$.

In this manuscript, we experimentally study the collective translational dynamics of a system of spinners (Fig. 1a) that are externally actuated in a quasi-2d air fluidized bed (Fig. 1b). Unlike colloidal spinners where the dynamics is governed by low Reynolds number, and hydrodynamic interactions are dominant [5,12], the collective translational dynamics in our system emerges from interparticle collisions and friction. Our spinners become translationally active through two distinct mechanisms: (i) As a result of perturbations caused by air flow, individual particles, while spinning, possess small translational Brownian motion with a narrow Gaussian distribution; (ii) When two spinners collide, some of their rotational energy is transformed to translational energy (and partially dissipated), and they jump apart at a greater relative speed, resulting in an avalanche of collisions which elevates translational activity. The latter mechanism contributes to non-Gaussian and ϕ-dependent $P(v)$s. In particular, we find that the shape of $P(v)$ strongly depends on the area fraction, ϕ, of the system. We then search for a thermodynamic description for the collective behavior manifested in translational degrees of freedom. We find a well defined effective equation of state with a surprisingly simple form that follows the hard sphere model.

Experiment

The spinner particles are disks of 1 cm in diameter and approximately 2 mm in thickness. A fan-like structure is embedded at the center of particles such that flow of air through the particles forces them to spin (Fig. 1a). The particles are 3D-printed using stereolithography technique (Projet 3500, 3D Systems) with 32 μm resolution, using VisiJet Crystal resin as the printing material.

The 3D-printed particles are placed on a sieve (mesh size of 150 μm) that is mounted on top of a custom-made wind box of size $0.5\times0.5\times1.2$ m^3 (Fig. 1b). Air is pumped to the bottom of the wind box, and passes through 1-inch-thick foam filter between two perforated metal sheets placed horizontally at the middle of the tower. More details on the setup are provided in [20–27]. An uniform upward air flow hits the particles placed on the sieve on top of the wind box and forces them to spin. For all of the experiments reported here, we maintain the air speed between 140 and 150 cm/s, which is lower than the levitation speed of the particles (~ 200 m/s), and high enough to overcome the rotational friction between the particles and the base. A round feature is printed on both sides at the center of the disks, to allow contact of spinning particles with the sieve. The rim of the particles on the other hand hover for most of the time. The particle rim occasionally hits the sieve and results in a transient reduction of spin rate (this effect may be pronounced during particle-particle collisions). As a result, our system of spinner particles resembles a granular gas in that an external source of energy maintains the dynamics, while the energy is dissipated by inelastic particle collisions and friction. By printing different particle geometries (in mass and fan pitch), as well as by slightly changing the air flow, we have obtained a range of angular speeds, from 26 to 41 revolutions per seconds (rps) (see Table 1). In this manuscript, we focus primarily but not exclusively on the collective dynamics of particles with the same spinning direction

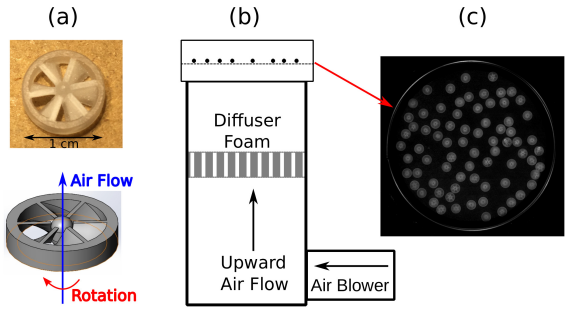

Fig. 1 (a) A spinner particle (1 cm diameter and 2 mm height) (b) Schematics of wind box setup (side view). (c) A sample image for area fraction $\phi = 0.3$. The particles spin on a sieve with mesh size of 150 μm. The air flow speed is 150 cm/s.

Spinners are illuminated from the top, and imaged using a high-speed digital camera (Phantom v7). The particles span 58 pixels in recorded images, and are identified and tracked using *trackpy*, a Python-based open source tracking software [43]. Images are taken at 67 frames per second for approximately 23 seconds of video for each experiment. Before recording each experiment, air is allowed to flow for 30 seconds so that the system reaches a steady state. The particles are confined to a circular area with diameter of either 20 cm or 15 cm (Fig. 1c). A rubber gasket is placed at the round edge of the confining region to avoid aggregation at the edge. The packing fraction is varied from $0.1 < \phi < 0.5$ by changing the number of particles (between 10 and 110 particles) and/or the size of the circular area.

Single-Particle Dynamics

We begin our analysis by describing the dynamics of a single spinning particle. The dynamics of four (4) randomly chosen particles from sample P4 (see Table 1) are shown in Fig. 2. The mean square displacement of single particles indicates ballistic motion (i.e. $\langle \Delta r^2(t) \rangle / d^2 \sim t^2$) for times $t < t^\star \simeq 0.1$ s (Fig. 2a). We use displacements associated with time lapse of $t^\star$ to extract translational velocities v. For all the data provided here, we have taken the single components of the velocity vector, v_x and v_y, where x

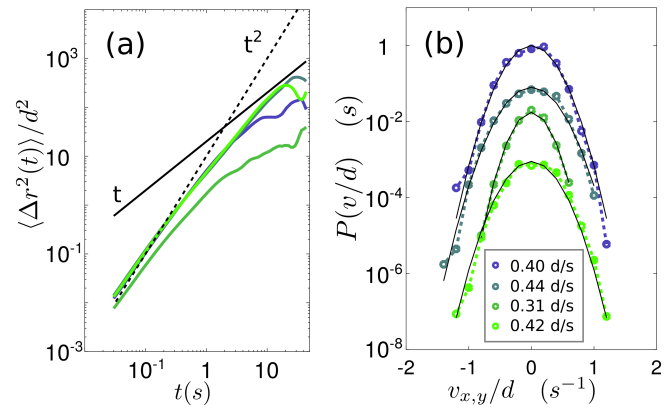

Fig. 2 Single-particle Dynamics: (a) Mean square displacement and (b) velocity distribution function for four randomly selected single particles from particle type P4. Each color represent one of the selected particles. The $P(v)$ data are shifted vertically axis for better visualization, and are well-fit to a normalized Gaussian function $P(v) = 1/\sqrt{2\pi v_g^2}\exp[-1/2(v/v_g)^2]$. The best fits are plotted by black curves for each distribution, and the associated fitting parameter, v_g, is provided in the inset (d is particle diameter). Although v_g has considerable variation over the randomly selected sample, the $P(v)$ for all of the tested particles demonstrate a Gaussian behavior.

and y are two arbitrary perpendicular directions. For an equilibrium system, velocity distributions $P(v)$ follows the Maxwell-Boltzmann distribution, and has Gaussian form. The variance of the Gaussian distribution is proportional to the thermodynamic temperature. As a system moves far from equilibrium, $P(v)$ becomes non-Gaussian. Fig. 2b shows that the translational velocity distributions for selected single particles (from particle type P4) have Gaussian distributions, and the translational dynamics of single spinners are effectively thermal. We also measure the angular speed of single particles for all particle types using a stroboscope. Measurements are performed for eight (8) randomly chosen particles from each particle type, and results are provided in Table 1. Having the single particle translational and angular speeds, we can calculate the ratio between translational and rotational energies as: $K_{\rm rot}/K_{\rm tr} = I\langle\omega^2\rangle/m\langle v^2\rangle$, where I is the moment of inertia with respect to rotating axis for the particles. The value of I should be very close to (but smaller than) the moment of inertia for a ring, which is $I = m(d/2)^2$. For instance, for particle type P4, $\sqrt{\langle v^2\rangle} = v_g \simeq 0.4\ d/s$, and $\sqrt{\langle\omega^2\rangle} \simeq \overline{\omega} = 26\ s^{-1}$. Hence, $K_{\rm rot}/K_{\rm tr} \simeq 1000$, which clearly indicates that the input of energy to the single particles is dominated by rotation.

Table 1 Specifications for printed spinners. The container diameter is 15 cm for particles P1, P3, and P4; and 20 cm for P2. All particles are 1 cm in diameter.

Type	Mass	Fan pitch	ω(rps)	Air Speed	Thickness
P1	0.114g	25°	39 ± 2	150 cm/s	2.5 mm
P2	0.092g	30°	41 ± 2	150 cm/s	2.1 mm
P3	0.092g	30°	33 ± 1	140 cm/s	2.1 mm
P4	0.111g	45°	26 ± 1	150 cm/s	2.2 mm

Multi-Particle Systems

In the next step, we characterize the translational velocity distribution $P(v)$ for a collection of spinners as a function of packing fraction ϕ. Velocity distributions of spinners for a few representative packing fractions are plotted for particle type P2 (Table 1) in Fig. 3a (Sample movies of multi-particle spinners are provided in the supplementary videos as Video1). The data shows that the shape of $P(v)$ strongly depends on ϕ. For a relatively low packing fraction, $\phi = 0.1$, we observe a central Gaussian-like distribution with width comparable to single particle behavior, and two heavy exponential tails. For a relatively high packing fraction case $\phi = 0.4$, on the other hand, the distribution is approximately (but not exactly) Gaussian. We believe that the anomalous ϕ-dependent shape of the velocity distributions is the result of interplay between the air-driven single-particle Brownian motion (Fig. 2b) and hyper-elastic particle collisions. At very low ϕ, the effects of these two mechanisms are decoupled both in time and energy scale. Single-particle dynamics contributes to the low energy central Gaussian shape of the distribution $P(v)$, while for higher velocities (the tails), which are associated with hyperelastic collisions, the distribution is exponential. As ϕ is increased, the interparticle collisions become more frequent, and the dynamics is dominated by hyperelastic jumps which is manifested by exponential distribution. Note that if two particles undergo a hyperelastic collision, their total translational kinetic energy increases after collision. In other words, the particles jump off each other after a collision with higher relative velocities. A relevant quantity to show the hyperelastic nature of collisions is the *coefficient of restitution*, $e = |\Delta\vec{v}'|/|\Delta\vec{v}|$. Here, $\Delta v'$ (Δv) is the relative velocity of the two colliding particles after (before) a collisional incident. An example of a typical collision (for system with $\phi = 0.1$) is shown in the supplementary videos as Video2. As seen, the particles jump off with a higher relative speed after the collision ($e \simeq 2$ in this example), which signifies hyperelastcity.

We note that the values of $K_{\rm rot}/K_{\rm tr}$ significantly decrease as ϕ increases, indicating that the rotational kinetic energy of the particles is partitioned into translational kinetic energy. For example, for particle type P4 at $\phi = 0.5$, we measure $\sqrt{\langle\omega^2\rangle} \simeq 4$ rounds/s and $\langle v^2\rangle = 1.4\ d^2/s^2$, which gives $K_{\rm rot}/K_{\rm tr} \simeq 2.8$. This ratio is approximately 3 orders of magnitude smaller than the corresponding ratio for a single particle ($K_{\rm rot}/K_{\rm tr} \simeq 1000$). Since the particles store less rotational kinetic energy as ϕ is increased, the hyperelastic collisions transfer less energy to translational mode. Hence, the collision-induced exponential shape of $P(v)$ spans smaller velocities, and the central Gaussian shape is gradually diminished (Fig. 3a).

Another important observation for our spinners is that, unlike translationally active systems which spatially self-organize in the form of giant number fluctuation and spontaneous phase separation[4,6–8,35,44], spinners remain spatially homogeneous. We verify the spatial homogeneity with measuring (particle) number fluctuation. To do so, we randomly select a circular subregion with radius r in a frame, and count the number of particles, N, within that region. We then find $\langle N\rangle$, and standard deviation of N, ΔN for numerous regions and by varying r. For a homogeneous sys-

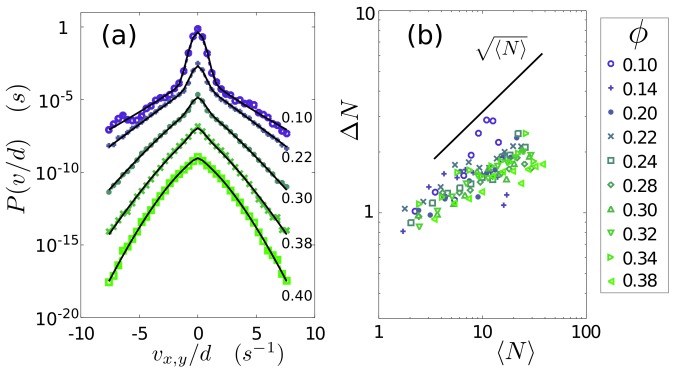

Fig. 3 Multi-Particle Systems: (a) Velocity distribution $P(v)$ for x component of particle velocities for packing fractions ϕ, 0.1, 0.2, 0.3, and 0.4. The data is provided for particles type P2. Similar behavior is observed for other particle types. (b) Number fluctuation (for particle type P2) as ϕ (inset) is varied. ΔN is the standard deviation of N. The solid line is $\Delta N = \sqrt{\langle N\rangle}$.

tem, one expects that the number fluctuations are Poissonian and scale as $\Delta N \sim \langle N\rangle^{1/2}$, while $\Delta N \sim \langle N\rangle$ in phase separating systems[44]. Fig. 3b shows that the number fluctuation measured for our spinners is consistent with a homogeneous system, and are actually somewhat sub-Poissonian. This observation is intriguing, since studies on active matter where the energy goes to the translational degrees of freedom report spatial inhomogeneity[8,44–46], even in the absence of hydrodynamic interactions[47]. In addition, note that ΔN grows slightly slower than $\langle N\rangle^{1/2}$. This observed sub-Poissonian statistics for number fluctuation is associated with an underlying structural order. For our non-crystalline and disordered system, a possibility of a hyperuniform structure exists. However, a systematic examination of hyperuniformity requires larger systems compared to our experimental data.

It is also important to note that, unlike results presented in[28], we do not observe correlated particle motion for the packing fractions we have explored. A possible explanation could be our distinctively higher rotational energy scales for single particles ($K_{rot}/K_{tr} \sim$1000), which results in hyperelastic collisions and subsequently destroys any possible correlated motion.

An Empirical Model for $P(v)$

In our system, an external source of energy (air flow) maintains the particle dynamics, while energy is dissipated by inelastic particle collisions and friction. As shown in Fig. 3a, we find non-Gaussian velocity distribution $P(v)$ for multi-particle systems (nearly Gaussian $P(v)$ are found for single-particle systems). Such non-Gaussian velocity distributions have been observed in granular gases, where $P(v)$ usually has a central form as $\exp[-|v|^{\alpha}]$ and tail forms as $\exp[-|v/v_c|^{\beta}]$ (The values of α and β depend on excitation mechanism)[15,19,38–42]. It is interesting to note that in some cooling states (where the energy input is turned off), a fully exponential distribution is observed[15,37]. These complex distributions were subject of comprehensive studies and were shown to agree with the prediction of modified Langevin equations[36,37]. In particular, Menzel and Goldenfeld[36] proposed a modified Langevin model with an added dry friction term (Coulomb friction), which is able to describe the anomalous vibrated granular gas $P(v)$. The solution form for $P(v)$ is a Gaussian term multiplied by an exponential term. However, the Menzel and Goldenfeld model did not capture our experimental $P(v)$ data very well.

Here, we propose an alternative empirical description, which captures the main features of our experimental $P(v)$ over a wide range of packing fractions. The proposed model is the sum of a Gaussian and a stretched exponential:

$$P(v) = (1-F)\frac{1}{\sqrt{2\pi v_g^2}} e^{-\frac{1}{2}(\frac{v}{v_g})^2} + F\frac{\beta}{2e^{v_e^{-\beta}}\Gamma(\frac{1}{\beta})} e^{-|\frac{v}{v_e}|^{\beta}} \qquad (1)$$

Here v_g and v_e are respectively the characteristic velocities associated with the Gaussian and stretched exponential distributions, and β is the stretching exponent. The relative importance of the two terms is given by the parameter F. In order to fit our $P(v)$ data to Eq. 1, we fix the value of v_g and fit the three remaining parameters, v_e, β, and F. The value of the characteristic velocity associated with the Gaussian distribution v_g is fixed at 0.50 d/s for all particle types, which corresponds to the best fit value for $P(v)$ for the lowest tested packing fraction (ϕ=0.1). The rationale for fixing v_g is the conjecture that the central Gaussian distribution is set by single-particle dynamics and the broadening is due to the hyperelastic collisions. Increasing the packing fraction, which decreases the average inter-collision time, should only decrease the *significance* of the Gaussian distribution but not its characteristic velocity, v_g. Hence, we expect that the characteristic v_g associated to single particle Brownian motion not to significantly change with ϕ. The fitted curves are shown by solid lines in Fig. 3a and show that Eq. 1 can capture our $P(v)$ data quite well for all of packing fractions. This agreement also verifies our initial conjecture on v_g being almost constant as a function of ϕ.

Results for the fitting parameters, F, β, and v_e are shown in Fig. 4 (left column) for all particle types (P1 - P4) as a function of ϕ. Note that the data for various particle types are quite scattered (except for parameter β). However, they as well as the physically measured quantity $\langle v^2\rangle$, collapse by scaling the packing fraction as $\phi \to (\phi - \phi^*)/\phi^*$ (Fig. 4 right column). Here, ϕ^* is the packing fraction where KE ($\langle v^2\rangle$) is maximum. For very low ϕ, as expected, the Gaussian form is dominant ($F \simeq 0$). As the packing fraction is increased, the contribution of exponential part also increases. At ϕ^*, the value of F/F^* is $\simeq$0.5 (between its two extreme limits, 0 and 1), which implies that both single particle and collisional dynamics play role in maximizing the translational KE. In other words, KE is maximized when there is sufficient interparticle collisions to maintain the translational activity, but the average collision frequency is low enough such that the single particles have enough time to regain their rotational speed and store energy in their highest capacity, and transfer higher energy to translational degrees in the subsequent collisions. It is also interesting to note that at ϕ^*, the value of β is approximately 1, which is associated with the fully exponential tails at intermediate ϕs. For very high packing fractions, β reaches 1.5, which is comparable to the vibrated granular gas counterpart[15,19,38–42].

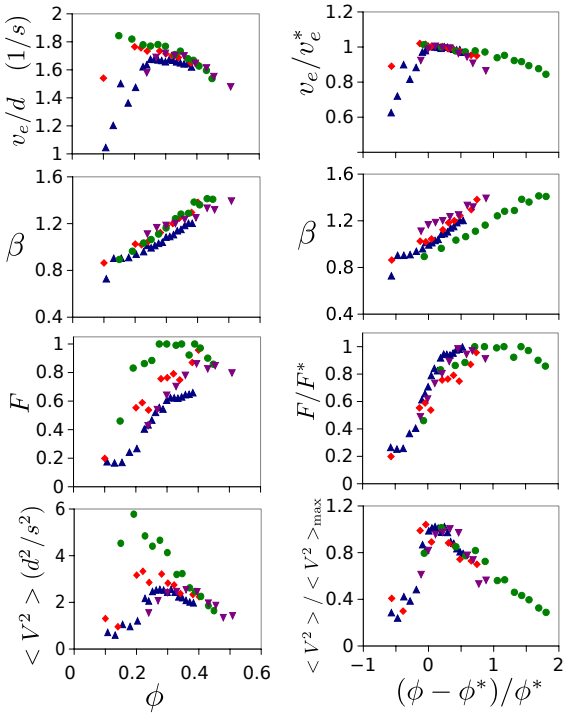

Fig. 4 Model fitting parameters: *Left Column*: Fitting parameters for $P(v)$ data as a function of ϕ; data is fitted to Eq. 1. Colors represent different particle types: blue: P1, red:P2, green:P3, and purple:P4. *Right Column*: Parameters v_e and F collapse by scaling the packing fraction by ϕ^* (see main text). The parameter β collapses before scaling the packing fraction. Here, v_e^* and F^* are respectively the values of v_e and F at ϕ^*, and ϕ^* is $= 0.25$ for P1, 0.23 for P2, 0.16 for P3, and 0.27 for P4. Similar collapse is also observed for average velocity squared.

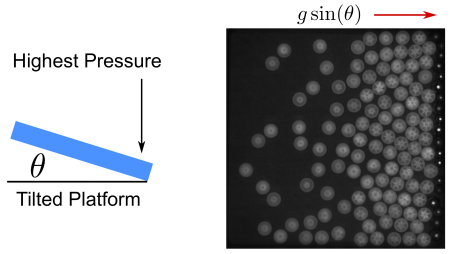

Fig. 5 A square shaped platform is used for thermodynamic measurements. The flat platform is tilted to arbitrary small angles θ in order to create pressure gradient through the system. Left: Side view schematics of tilted platform. Right: A sample image of the particles in tilted platform. The effective gravity direction is towards the right of the image. A layer of steal bars are added to the right side to create a rough surface at the base.

Equation of State

Describing active systems using classical thermodynamics is a challenge since such systems are inherently out of equilibrium. In equilibrium systems, a well-defined equation of state exists which describes the relationship between macroscopic extensive quantities (pressure p, temperature T, and density or packing fraction ϕ). Recently, it has been argued[48] that pressure is not a well-defined quantity for active systems and therefore an equation of state may not be attainable, with the exception for systems in which particle interactions are isotropic[4]. The majority of past works focus mainly on the consequence of translational activity. Here, on the other hand, we search for the existence of an equation of state for our system of spinners, where the translational dynamics is obtained through rotational activity. To measure temperature, pressure and density, we follow the procedure outlined in[27]. In short, the platform (Fig.1b) is tilted to various small angles θ, which creates a pressure gradient through the system (Fig. 5). We use a square shaped container with edge size of $L = 16$ cm for this procedure. A sample video of the experiment is provided in the supplementary videos (Video3). We then measure the mean-square speed at slices equivalent to two particle diameters and perpendicular to effective gravity direction. The effective temperature is defined as $k_B T_{\rm eff} = m\langle v^2 \rangle$. The hydrodynamic pressure is given for each slice as $p = Nmg\sin\theta/L$, where N is the number of particles residing above each slice; and the packing fraction is simply defined as the area spanned by particles at each slice.

Fig. 6 shows the computed dimensionless pressure, $Z = pd^2/k_B T_{\rm eff}$ as a function of ϕ. Note that the quantity Z is measured for all particle types and several tilt angles. The data for all measurements collapse onto a single curve, indicating that a well-defined equation of state exists for our spinners. We fit the experimental data to the prediction for a free volume model of 2D hard spheres given by $Z \propto \phi/(1-(\phi/\phi_c)^{1/2})$[49]; fit is the solid line in Fig. 6. We note that the value of $\phi_c = 0.81$ from the fit is close to the jamming point packing fraction, $\phi_J \simeq 0.84$.

Searches for Exotic Behavior

(i) *Segregation dynamics for mixture of CW and CCW spinners:* Previous numerical studies[35,50] demonstrated that in mixtures of particles with opposite spin direction (i.e. CW and CCW rotating particles), local or large scale regions of particles with similar spin direction form. In search for an experimental analogue, we printed particles which were mirror images of the original tested particles, and studied the dynamics of the mixture. We observe that small regions of CW or CCW particles temporarily form and quickly dissolve (See a sample movie in the supplementary video, Video4). Note that our experimental container area is much smaller than the studied area in[35]. The possibility of spin-segregation for larger areas remains for future investigations.

(ii) *Dynamics of spinners with added geometrical friction:* As we described in details in previous sections, the dynamics of active spinners resemble a near-equilibrium system. Note that the friction between particles is non-zero (yet very small), which partially contribute to transformation of rotational energy to transla-

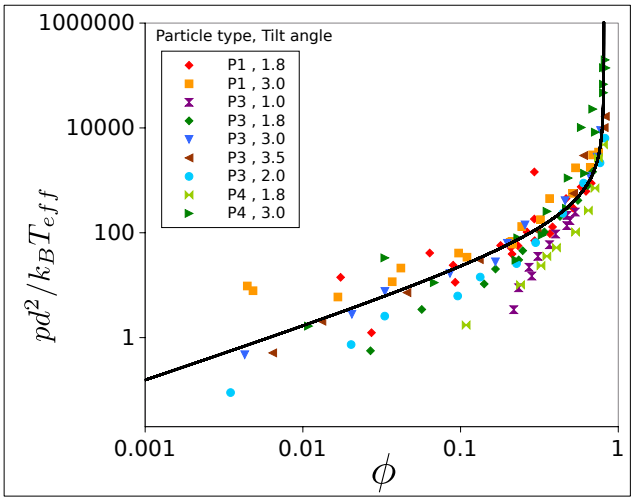

Fig. 6 Dimensionless pressure, $Z = pd^2/k_BT_{\text{eff}}$, vs. packing fraction, ϕ for tilt angles between 1° and 3.5°. The solid line is the fitted curve to equation $Z = C\phi/(1-(\phi/\phi_c)^{1/2})$, with $C = 150$, and $\phi_c = 0.81$.

tional energy during inelastic collisions. In search for the effects of increasing particle-particle friction on the overall dynamics, we added geometrical friction to particles by including small features (bumps) to the rims of particles (See supplementary video, Video5). We observe that by adding geometrical friction, the system becomes spatially inhomogeneous, and stable solid regions form which coexist with the highly active gas phase. In future, we will study the effects of this added friction on the existence of an equation of state.

(iii) *Swarming was never observed:* This was searched for with different container geometries and boundary conditions but not found.

Conclusions

In conclusion, we experimentally investigated the dynamics and thermodynamic properties of a system of active spinners driven by air flow. We found that while single particle dynamics demonstrate nearly Gaussian velocity distribution $P(v)$ (Fig. 2b), multiparticle systems show $P(v)$ that strongly depended on ϕ and have heavy tails much stronger than for typical granular gases (Fig. 3a). Unlike translationally active systems, our spinners remained spatially homogeneous (Fig. 3b). An empirical model based on the sum of a Gaussian and stretch exponential statistics (Eq. 1) was able to capture the functional forms of the multiparticle $P(v)$. We finally measured the equation of state for our system of spinners and showed that even though the system is dissipative and particles exhibit complex and non-trivial interactions, the thermodynamics of spinners is effectively similar to thermal hard spheres. A remarking feature of our experiment is its ability to explore relatively high rotational energy inputs (ωs as high as 40 rps were achieved). A possible explanation for observing a near-equilibrium effective thermodynamics is that the particles act as almost infinite local energy sources. As a result, any amount of translational energy loss (through friction and inelastic collisions) is instantly regained in the form of rotational energy, and subsequently partitions to the translational degrees.

In future, we will discuss the spin-segregation of clockwise and counterclockwise mixtures as well as the dynamics of particles with added geometrical friction (by adding bumps to particle rim).

Acknowledgements

This work was supported by NSF grants MRSEC/DMR-1120901, DMR-1305199 (DJD), and REU-Site DMR-1359351.

Notes and references

1 M. C. Marchetti, J. F. Joanny, S. Ramaswamy, T. B. Liverpool, J. Prost, M. Rao and R. A. Simha, *Rev. Mod. Phys.*, 2013, **85**, 1143.
2 H. H. Wensink, J. Dunkel, S. Heidenreich, K. Drescher, R. E. Goldstein, H. Löwen and J. M. Yeomans, *Proc. Natl. Acad. Sci.*, 2012, **109**, 14308.
3 A. Bricard, J.-B. Caussin, D. Das, C. Savoie, V. Chikkadi, K. Shitara, O. Chepizhko, F. Peruani, D. Saintillan and D. Bartolo, *Nat. Commun.*, 2015, **6**, 7470.
4 A. P. Solon, J. Stenhammar, R. Wittkowski, M. Kardar, Y. Kafri, M. E. Cates and J. Tailleur, *Phys. Rev. Lett.*, 2015, **114**, 198301.
5 B. Grzybowski, H. Stone and G. M. Whitesides, *Nature*, 2000, **405**, 1033.
6 M. E. Cates and J. Tailleur, *Annu. Rev. Condens. Matter Phys.*, 2015, **6**, 219.
7 F. Ginot, I. Theurkauff, D. Levis, C. Ybert, L. Bocquet, L. Berthier and C. Cottin-Bizonne, *Phys. Rev. X*, 2015, **5**, 011004.
8 I. Buttinoni, J. Bialké, F. Kümmel, H. Löwen, C. Bechinger and T. Speck, *Phys. Rev. Lett.*, 2013, **110**, 238301.
9 J. Palacci, C. Cottin-Bizonne, C. Ybert and L. Bocquet, *Phys. Rev. Lett.*, 2010, **105**, 088304.
10 B. C. van Zuidena, J. Paulosea, W. T. M. Irvine, D. Bartolod and V. Vitelli, *PNAS*, 2016, **113**, 12919–12924.
11 B. Delmotte, M. Driscoll, P. Chaikin and A. Donev, *Phys. Rev. Fluids*, 2017, **2**, 092301(R).
12 M. Driscoll, B. Delmotte, M. Youssef, S. Sacanna, A. Donev and P. Chaikin, *Nat. Phys.*, 2017, **13**, 375.
13 A. Puglisi, V. Loreto, U. M. B. Marconi, A. Petri, and A. Vulpiani, *Phys. Rev. Lett.*, 1998, **81**, 3848.
14 D. L. Blair and A. Kudrolli, *Phys. Rev. E*, 2003, **67**, 041301.
15 W. Losert, D. G. W. Cooper, J. Delour, A. Kudrolli and J. P. Gollub, *Chaos*, 1999, **9**, 682.
16 V. Narayan, S. Ramaswamy and N. Menon, *Science*, 2007, **317**, 105–108.
17 M. Baur and K. Huang, *Phys. Rev. E*, 2017, **95**, 030901(R).
18 R. Brito and M. H. Ernst, *Europhys. Lett.*, 1998, **43**, 497–502.
19 M. G. Clerc, P. Cordero, J. Dunstan, K. Huff, N. Mujica, D. Risso and G. Varas, *Nat. Phys.*, 2008, **4**, 249.
20 R. P. Ojha, P. A. Lemieux, P. K. Dixon, A. J. Liu and D. J. Durian, *Nature*, 2003, **427**, 521.
21 R. P. Ojha, A. R. Abate and D. J. Durian, *Phys. Rev. E*, 2005, **71**, 016313.

22 A. R. Abate and D. J. Durian, *Phys. Rev. E*, 2005, **72**, 031305.

23 A. R. Abate and D. J. Durian, *Phys. Rev. Lett.*, 2008, **101**, 245701.

24 L. J. Daniels, Y. Park, T. C. Lubensky and D. J. Durian, *Phys. Rev. E*, 2009, **79**, 041301.

25 L. J. Daniels and D. J. Durian, *Phys. Rev. E*, 2011, **83**, 061304.

26 M. E. Beverland, L. J. Daniels and D. J. Durian, *J. Stat. Mech.*, 2011, **2011**, P03027.

27 L. J. Daniels, T. K. Haxton, N. Xu, A. J. Liu and D. J. Durian, *Phys. Rev. Lett.*, 2012, **108**, 138001.

28 M. Workamp, G. Ramirez, K. E. Daniels and J. A. Dijksman, *arXiv*, 2018.

29 H. M. López, J. Gachelin, C. Douarche, H. Auradou, and E. Clément, *Phys. Rev. Lett.*, 2015, **115**, 028301.

30 B. J. Nelson, I. Kaliakatsos and J. J. Abbott, *Ann. Rev. Bioeng.*, 2010, **12**, 55–85.

31 C. Bechinger, R. D. Leonardo, H. Löwen, C. Reichhardt, G. Volpe and G. Volpe, *Rev. Mod. Phys.*, 2016, **88**, 045006.

32 E. Lushi and P. M. Vlahovska, *J. Nonlinear Sci.*, 2015, **25**, 1111.

33 R. Cafiero, S.Luding and H. J. Herrmann, *Europhys. Lett.*, 2002, **60**, 854.

34 C. Scholz and T. Pöschel, *Phys. Rev. Lett.*, 2017, **118**, 198003.

35 N. H. P. Nguyen, D. Klotsa, M. Engel and S. C. Glotzer, *Phys. Rev. Lett.*, 2014, **112**, 075701.

36 A. M. Menzel and N. Goldenfeld, *Phys. Rev. E*, 2011, **84**, 011122.

37 A. Kawarada and H. Hayakawa, *J. Phys. Soc. Jpn.*, 2004, **73**, 2037.

38 J. C. Burton, P. Y. Lu and S. R. Nagel, *Phys. Rev. E*, 2013, **88**, 062204.

39 J. S. Olafsen and J. S. Urbach, *Phys. Rev. Lett.*, 1998, **81**, 4369.

40 T. Antal, M. Droz and A. Lipowski, *Phys. Rev. E*, 2002, **66**, 062301.

41 K. Harth, U. Kornek, T. Trittel, U. Strachauer, S. Höme, K. Will and R. Stannarius, *Phys. Rev. Lett.*, 2013, **110**, 144102.

42 S. Tatsumi, Y. Murayama, H. Hayakawa and M. Sano, *J. Fluid Mech.*, 2009, **641**, 521–539.

43 `http://dx.doi.org/10.5281/zenodo.34028`.

44 Y. Fily and M. C. Marchetti, *Phys. Rev. Lett.*, 2012, **108**, 235702.

45 J. Bialké, H. Löwen and T. Speck, *EPL*, 2013, **103**, 30008.

46 J. Schwarz-Linek, C. Valeriani, A. Cacciuto, M. E. Cates, D. Marenduzzo, A. N. Morozov and W. C. K. Poon, *Proc. Nat. Acad. Sci.*, 2012, **109**, 4052.

47 J. Tailleur and M. E. Cates, *Phys. Rev. Lett.*, 2008, **100**, 218103.

48 A. P. Solon, Y. Fily, A. Baskaran, M. E. Cates, Y. Kafri, M. Kardar and J. Tailleur, *Nat. Phys.*, 2015, **11**, 673.

49 C. D. Modes and R. D. Kamien, *Phys. Rev. E*, 2008, **77**, 041125.

50 M. Spellings, M. Engel, D. Klotsa, S. Sabrina, A. M. Drews, N. H. P. Nguyene, K. J. M. Bishop and S. C. Glotzer, *Proc. Nat. Acad. Sci.*, 2015, **112**, E4642–E4650.